ARTICLE

Controlled Fabrication of Fluorescent Barcode Nanorods

Xiao Li, Tieqiang Wang, Junhu Zhang,* Difu Zhu, Xun Zhang, Yang Ning, Hao Zhang, and Bai Yang

State Key Laboratory of Supramolecular Structure and Materials, College of Chemistry, Jilin University, Changchun 130012, P. R. China

ABSTRACT We report a novel technique for generating polymer fluorescent barcode nanorods by reactive ion etching of polymer multilayer films using nonclose-packed (ncp) colloidal microsphere arrays as masks. The fluorescent polymer multilayer films were spin-coated on a substrate, and ncp microsphere arrays were transferred onto these films. The exposed polymers were then etched away selectively, leaving color-encoded nanorods with well-preserved fluorescent properties. By modifying the spin-coating procedure, the amount of polymer in each layer could be tuned freely, which determined the relative fluorescence intensity of the barcode nanorods. These nanorod arrays can be detached from the substrate to form dispersions of coding materials. Moreover, the shape of the nanorods is controllable according to the different etching speeds of various materials, which also endows the nanorods with shape-encoded characters. This method offers opportunities for the fabrication of novel fluorescent barcodes which can be used for detecting and tracking applications.

KEYWORDS: fluorescent barcode · multisegments · nanorod · microarray · colloidal lithography

Encoded nanomaterials, with a large number of readily distinguishable barcode patterns, are particularly attractive for their important applications, ranging from product tracking to multiplexed biodetection.[1−3] Unlike barcode identifiers of adjacent black and white lines that are visible to the naked eye, encoded nanomaterials are extremely desirable as an invisible tag for valuable products or classified information. The widespread use of barcode nanomaterials requires high coding capacity, low-cost large-scale particle production, and a portable and accurate detection system.[4] Facing these demands, many techniques for designing barcoded nanomaterials have been developed. Porous membranes have been used as templates for the preparation of encoded metal nanowires with a large number of distinguishable patterns. The nanowires constructed within the templates were obtained through electrochemical reduction of metal ions from solutions by using multiple plating baths to deposit sequential segments of different metals,[5−8] or a single plating solution containing multiple types of metallic ions with differing reduction potentials.[9,10] Employing a similar deposition route and sacrificial layers, linear chains of Au and Ag nanoparticles can be created.[11,12] Nanomaterial-based barcode systems have also been constructed by anisotropic growth of heterometallic nanorods without hard templates,[13] or direct end-to-end assembly of Au/Pt/Au multisegmented nanowires using the biotin/avidin linkage,[14] and layer-by-layer assembly of multicomponent nanoparticle arrays using supramolecular forces.[15] However, the detection of heterostructured nanowires based on the reflectivity difference of the component metals may be disturbed by the reflectance of background or environment resulting in poor identifications.

Compared with the metal barcodes,[16] fluorescent barcodes are becoming more important because of their straightforward detection and quantification of the encoding difference using fluorescence as the output signal. By taking advantage of the well-known surface coordination chemistry, multicomponent metal nanowires were selectively functionalized with organic molecules that could be quantified by fluorescence microscopy.[17,18] Improved one-step template-guided electrodeposition has been applied to fabricate alloy nanowires with distinct X-ray fluorescence barcode patterns.[19] Optically encoded diffractive barcodes fabricated from SU-8 can also be used as fluorescence assays, using the functionality of probe biomolecules as identifiers.[20,21] However, few choices of materials and time-consuming synthesis are the major problems of these techniques. Recently, there have been many developments leading to an increase in the activity

*Address correspondence to zjh@jlu.edu.cn.

Received for review November 27, 2009 and accepted July 19, 2010.

Published online July 27, 2010.
10.1021/nn9017137

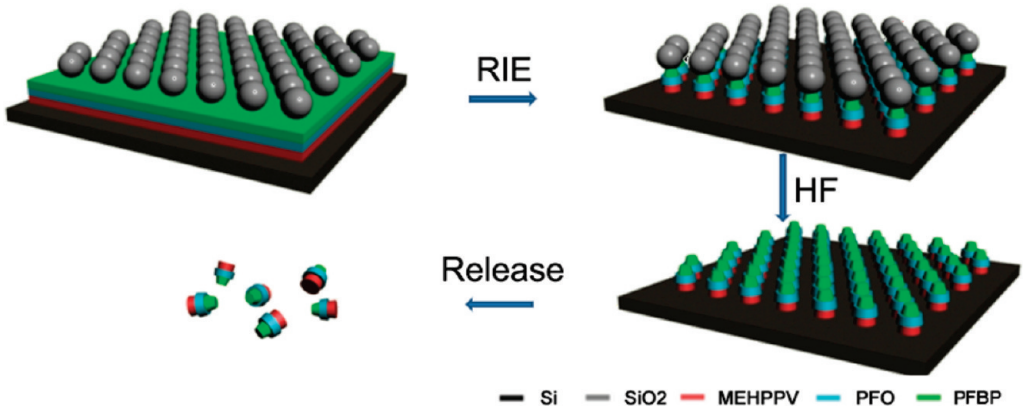

Figure 1. The schematic illustration for the fabrication of fluorescent nanorod arrays *via* RIE and the further release of nanorods from the substrate by HF etching.

on optical "barcoding" that are mainly based on the use of rare-earth doped glass,[22] fluorescent silica colloids,[23−25] oligonucleotide-linked colloidal gold,[26] and the incorporations of semiconductor quantum dots (QDs) into microbeads[27−31] or hydrogel spheres.[32] Compared with spheric barcodes, nanorods are a more interesting class of materials because the length of rods allows for massive encoding and functionalization with conventional surface chemistry strategies. Therefore, introducing the important factors of the "rod" into a fluorescent barcode can effectively improve the capacity of coding and signal output. It is still a challenge to obtain multicolor fluorescent nanorods with controllable size *via* simple and inexpensive technologies.

Herein, we developed a novel technique for fabricating ordered arrays of fluorescent polymer barcode nanorods *via* reactive ion etching (RIE) with colloidal masks. With the help of layer after layer spin-coating, we prepared multilayered polymer films with distinguishable fluorescent properties on flat substrates. By utilizing the lift-up and transfer-printing method we reported previously,[33] two-dimensional (2D) nonclose-packed (ncp) colloidal microsphere arrays were transferred onto the surface of the multilayered films.[34] After a mask-directed RIE process, color-encoded multisegmented nanorods were obtained. The thicknesses of each layer were tuned by changing the spin-coating conditions. Accordingly, the proportions of each component in the nanorods were also adjusted optionally. Furthermore, the arrays of nanorods were released to water and formed suspensions as coding materials. These color-encoding nanorods with different composition or shape patterns have a broad range of applications, such as product tracking and protection to bioassays.[35]

RESULTS AND DISCUSSION

Fabrication of Poly(*p*-phenylene vinylene) (PPV) Nanorods by Reactive Ion Etching (RIE) with Colloidal Masks. The overall fabrication process is schematically depicted in Figure 1. First, fluorescent polymer multilayers which incorporated different components in each layer were fabricated by spin coating. By employing solvent-swelling and a transfer-printing process,[33,34] ncp microsphere arrays were transferred to the surface of the polymer film. Subsequently, the exposed polymers were etched away selectively *via* RIE, leaving color-encoded nanorods with well-preserved fluorescent properties under the microspheres on the substrate. After dissolving the microspheres in a hydrofluoric acid (HF) solution, ncp multisegmented nanorod arrays were obtained on the substrate. By further dissolving the SiO_2 layer between the substrate and the fluorescent polymer, the nanorods were released into the solution.

To prove the feasibility of our method, we performed the fabrication process on a monolayer of fluorescent polymer. PPV precursor film was prepared by spin-coating an aqueous solution of the precursor polymer (poly(*p*-xylene tetrahydrothiophenium chloride)) onto a silicon substrate, and then heated at 300 °C under a nitrogen atmosphere for 2 h to convert the precursor to PPV without thermal damage.[36] A monolayer of ncp silica microspheres acting as masks was then transferred onto the surface of PPV. During the RIE process, the PPV in the space between the microspheres was exposed to radical ion fluid. It should be noted that compared with close-packed microsphere arrays, the larger voids of ncp microspheres allowed for a better penetration of radical ions and generation of individual nanorod. Therefore, these unprotected areas were gradually etched away, leading to PPV nanorods with microspheres on top. After removing the silica micospheres with HF, PPV nanorod arrays were fabricated on the substrate. The nanorod arrays were then cleaned by dipping and rinsing in deionized water for several cycles.

Scanning electron microscope (SEM) images displayed in Figure 2a and 2b show the cross-sectional view of nanorod arrays before and after removal of the microspheres, respectively. These images indicate that neither the HF-etching nor the cleaning process had any influence on the shape or quality of the nanorod

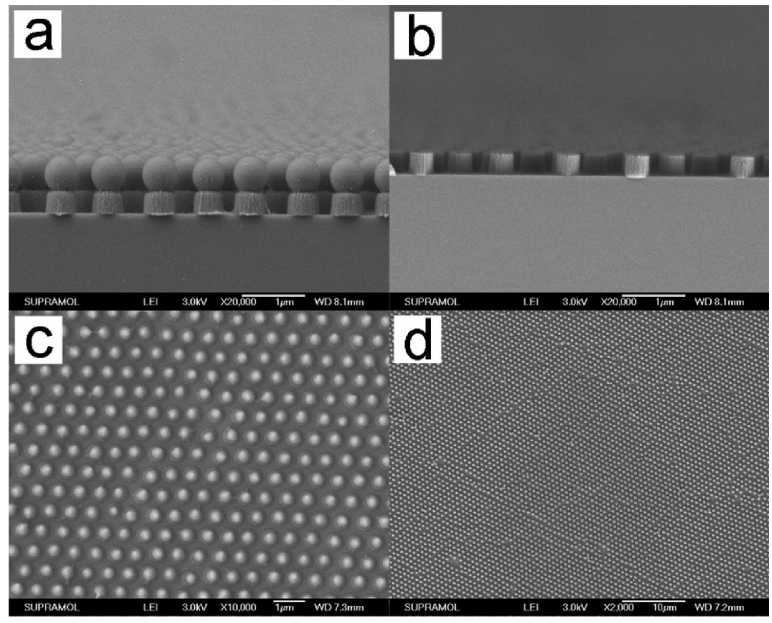

Figure 2. SEM cross-section images of the PPV nanorod arrays with silica microspheres (a) and after removal of the silica microspheres (b); high (c) and low-magnification (d) top-view SEM images of the hexagonal arrays of PPV nanorods.

arrays. Careful observation reveals that the diameters of the nanorods were slightly smaller than that of the silica microspheres above them. This difference can be explained by the nature of etching process. The extensive energetic gaseous molecule bombarded on the masks and scattered in all directions. Longer etching time allowed the etching molecules to diffuse or scatter into the gaps between the masks and the polymers surface, leading to the removal of polymer clusters underneath the masks and the generation of increased horizontal etching under the masks.[37,38] The top view SEM images of the oriented nanorod arrays shown in Figure 2c,d demonstrate the regularity and the well preserved long-range ordering (more than 100 μm^2) that can be routinely achieved by our method.

Figure 3 gives the optical (a) and fluorescent (b) microscopy micrographs of the PPV nanorod arrays. The fluorescent image (Figure 3b) was taken from the

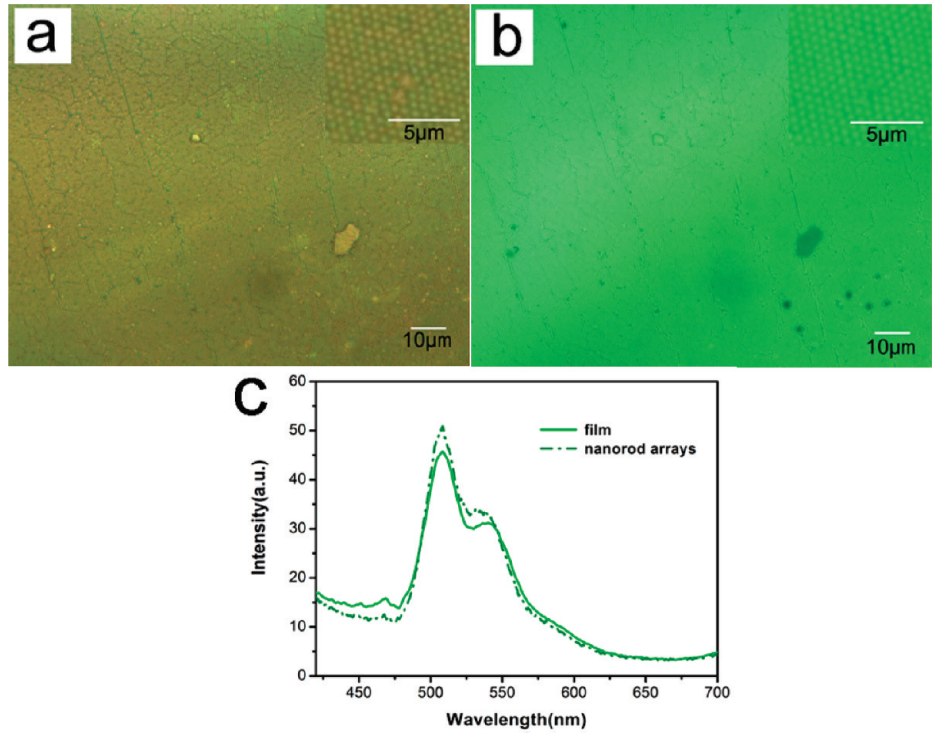

Figure 3. Optical microscopy (a) and fluorescence microscopy (b) images of PPV nanorod arrays. (c) PL emission spectra from PPV film and PPV nanorods arrays.

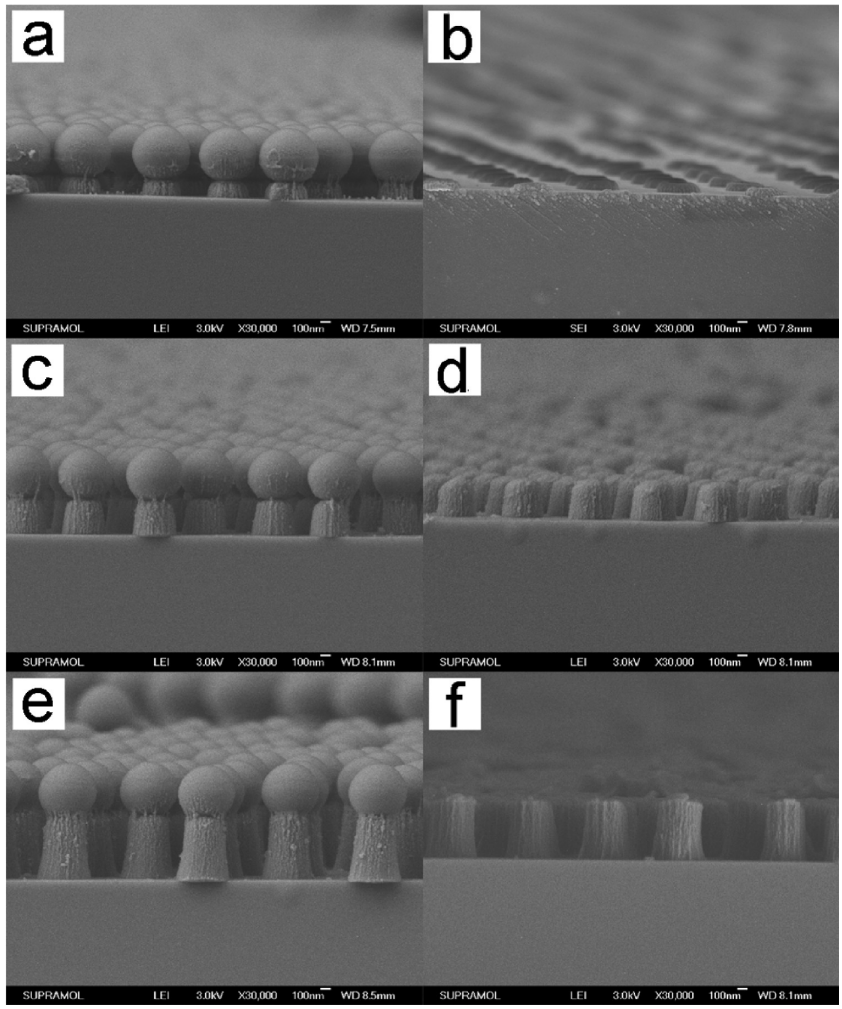

Figure 4. SEM images of PPV nanorods with different heights before (a, c, e) and after (b, d, f) etching the silica microspheres.

same area in Figure 3a, and the PPV nanorods showed green photoluminescence under excitation. In addition, the photoluminescence (PL) spectra of the PPV film before and after the RIE procedure are shown in Figure 3c. No obvious fluorescent peak shift was observed. Moreover, the spectral shape of PPV remained unchanged after the RIE and HF-etching steps.

An important factor of barcoding, the height of PPV bars, that is, the thickness of the PPV film, can be easily adjusted by changing the spinning rate and the concentration of polymer solution, which agreed well with the simple model of spin coating.[39] By fixing the spinning rate and neglecting the solvent evaporation during the spinning process, the film thickness is directly proportional to the concentration in a moderate concentrated solution.[40] As indicated in Figure 4, by tuning the concentrations of precursor polymer solution and appropriate etching durations, nanorod microarrays with different heights were successfully obtained (130, 300, and 610 nm in Figure 4a−f, respectively). The controllable height of the nanorods provides opportunities for fabricating accurate multisegmented barcode nanorods.

Fabrication of Multisegmented Nanorods with Controllable Morphologies. Multisegmented nanorod arrays were fabricated by spin-coating multilayered polymer films with different fluorescent colors. A big challenge of spin-coating multilayer film is solvent dissolution, which will damage the preceding layers. The optimal case is that the solvent for the following layer is a poor solvent for the preceding layer. For example, we successively spin-coated a PVA@PPV film (the mass proportion of poly(vinyl alcohol) (PVA) and PPV precursor was 99:1) on the top of PPV layer, as deionized water is a good solvent for PVA@PPV, but a bad solvent for PPV. The SEM images in Figure 5 show the bilayer PPV/PVA@PPV nanorods after RIE. The PPV and PVA@PPV segments were distinguished by the boundary. The average heights of the PPV and PVA@PPV segments were *ca.* 300 and 900 nm, respectively. The nanorods had a smaller head and a broader tail, which was a typical sign of undercut effect during RIE.[37,38] PL emission spectra were used to characterize the barcoding capability of our barcode nanorods (Figure 5c). The green-emission peak in the spectrum suggested that the PPV maintained the same optical characteristics before and

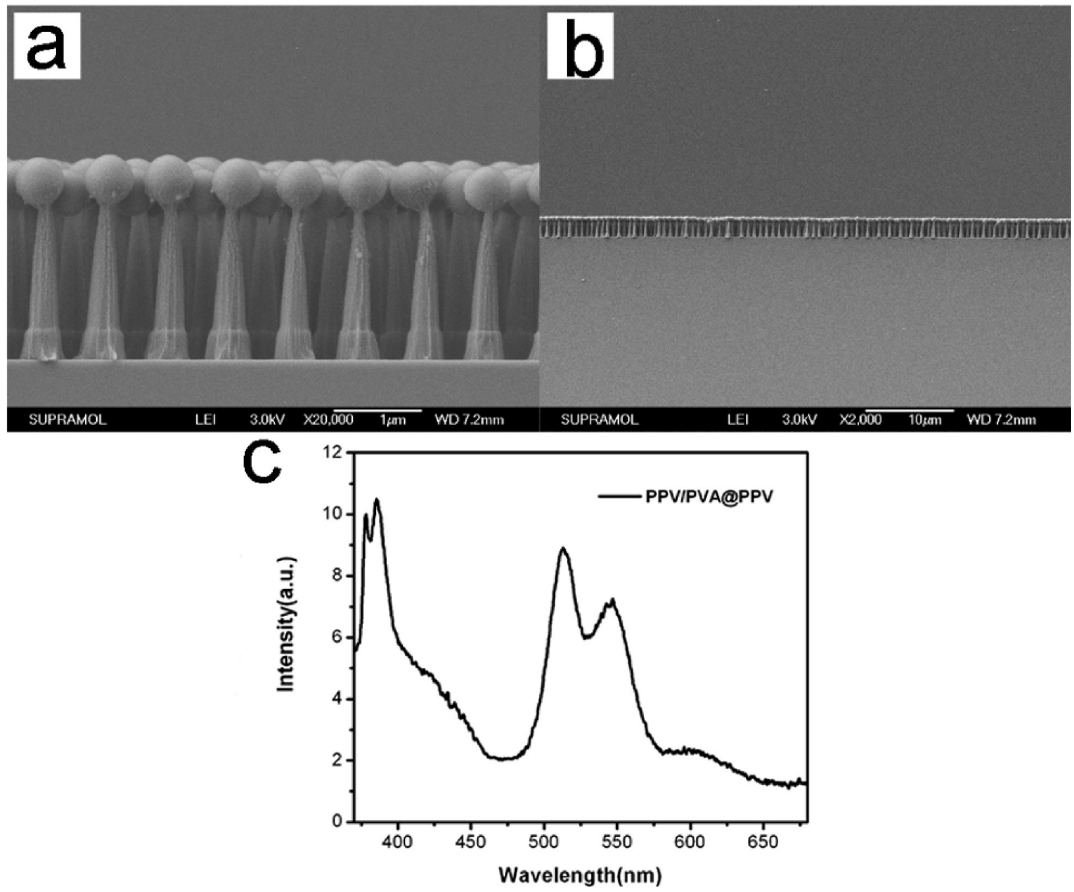

Figure 5. High and low magnification SEM images of PPV/PVA@PPV two-layered barcode nanorods (a, b); PL emission spectrum of PPV/PVA@PPV nanorods (c).

after the etching process. A blue-emission peak at 380 nm for the blend of PVA@PPV was also observed. This is because the fluorescence spectrum of PPV is very sensitive to the amount of blended PVA, which is consistent with the literature reported by Chen *et al.*[41]

The data density of linear barcodes can be predicted by $(m^n + m^{\mathrm{ceil}(n/2)})/2$ (eq 1), where m is the number of lines (or bit), and n is the types of lines.[42] To increase the data capacity of our barcode nanorods without increasing the number of layers, we introduced three PL polymers with different emission colors as building blocks. Three fluorescent polymers, poly(9,9-dihexylfluorene-2,7-diyl)-*co*-alt-(dibenzo[a,c]phenazine) (PFBP), poly(9,9′-dioctyl-9*H*-fluorene-2,7-diyl) (PFO), and poly[2-methoxy-5-(2′-ethylhexyloxy)-1,4-phenylenevinylene] (MEHPPV) were employed. The chemical structures of PFBP, PFO, and MEHPPV are given in Chart 1. MEHPPV, PFBP, and PFO shows red (576 nm), green (500 nm), and blue (440 nm) PL emission, respectively (Figure 6b). Compared with the absorption spectra, the emission wavelengths of PFBP and PFO were within the absorption spectra of MEH-PPV (Figure 6a). To prevent the upper layer from absorbing the emission of the lower layer, the MEHPPV layer was set at the bottom in this system to allow for more accurate barcoding. The sequence between the PFBP and PFO layers is switchable as no absorption interference between PFBP and PFO was observed.

Tricolor barcode nanorods with different codes were prepared by spin-coating the fluorescent polymers with different sequences. To avoid the solvent dissolution, these three oil-soluble polymers were separated by thin nonfluorescent water-soluble PVA layers. SEM images of the nanorods in Figure 7a,b show the

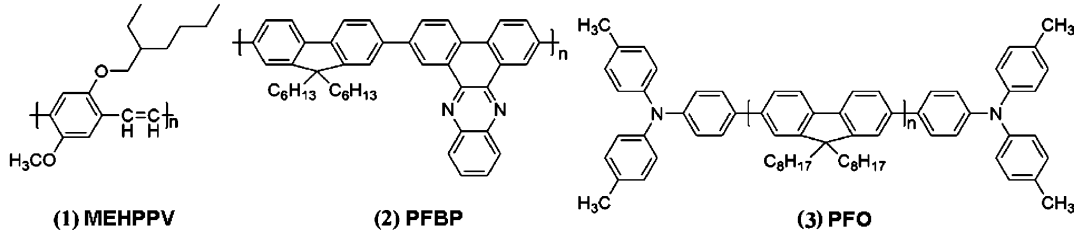

Chart 1. Chemical Structures of MEHPPV (Red Emission), PFBP (Green Emission), and PFO (Blue Emission)

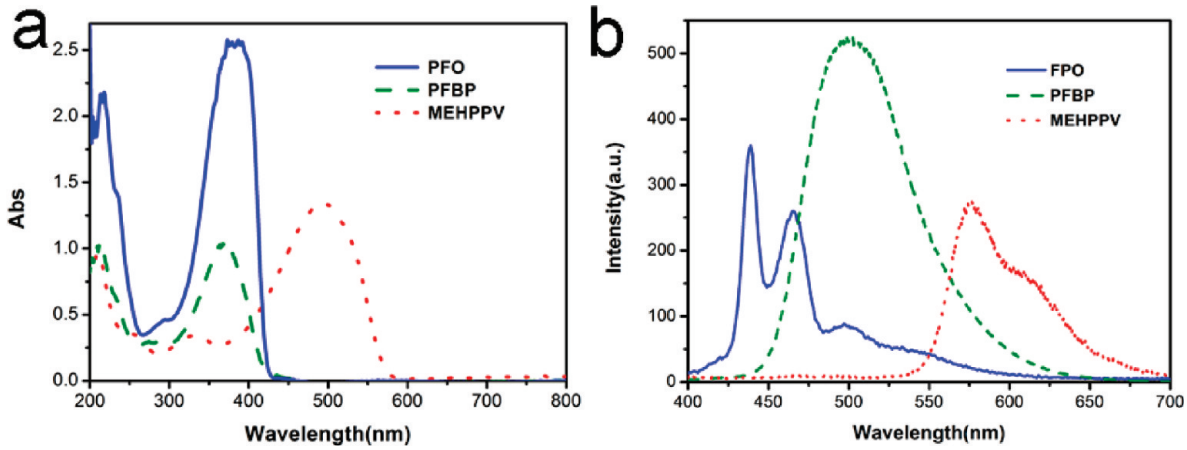

Figure 6. UV−visible absorption spectroscopy of MEHPPV, PFO, and PFBP films (a); PL emission spectra of MEHPPV, PFO, and PFBP films (b). The excitation wavelength used for these spectra was 350 nm.

multisegmented nanorods with the sequences (top to bottom) of PFO/PFBP/MEHPPV (blue/green/red) and PFBP/PFO/MEHPPV (green/blue/red), respectively. Both types of the multisegment nanorods remained standing

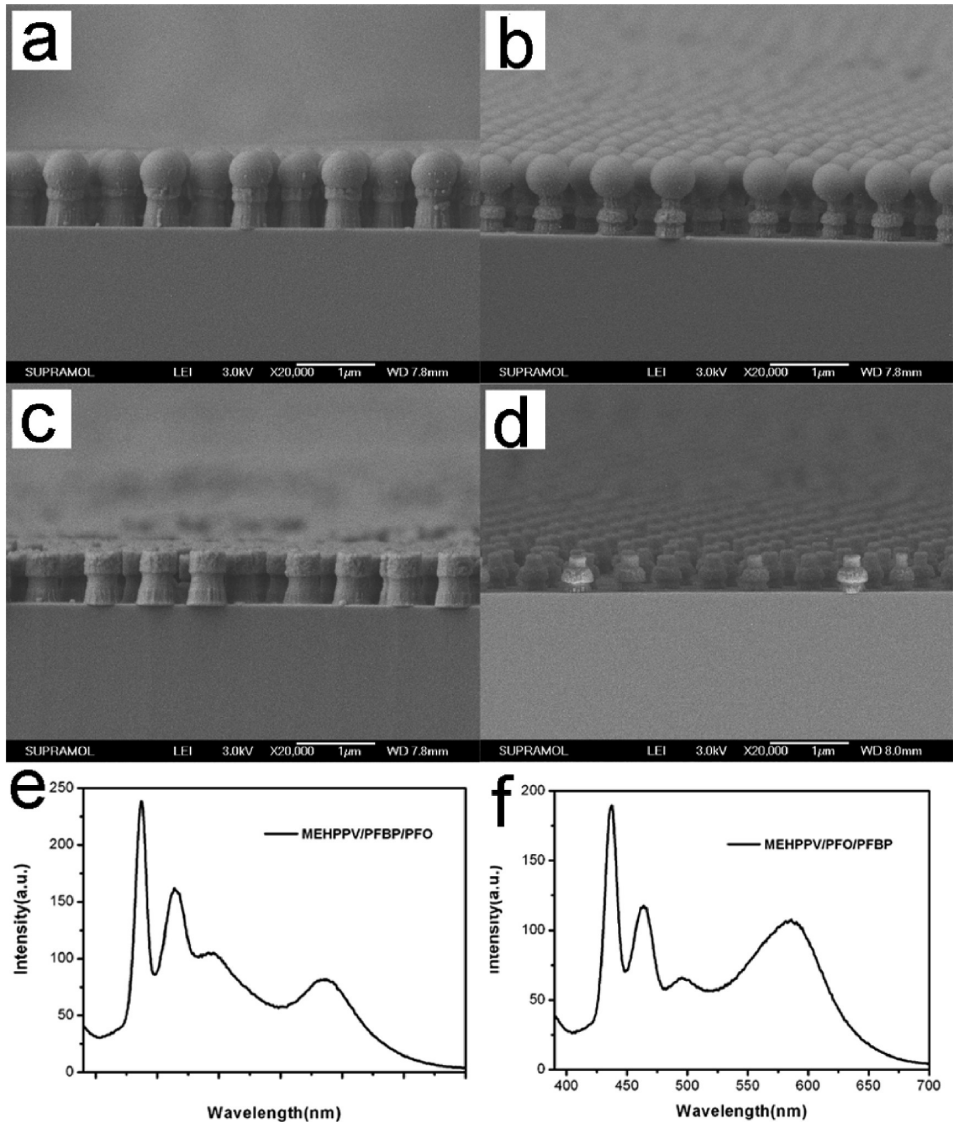

Figure 7. SEM images of MEHPPV/PFBP/PFO nanorods (a) before and (c) after the removal of the silica microspheres and (e) the corresponding PL emission spectrum; SEM images of MEHPPV/PFO/PFBP nanorods (b) before and (d) after removing the silica microspheres and (f) the corresponding PL emission spectrum.

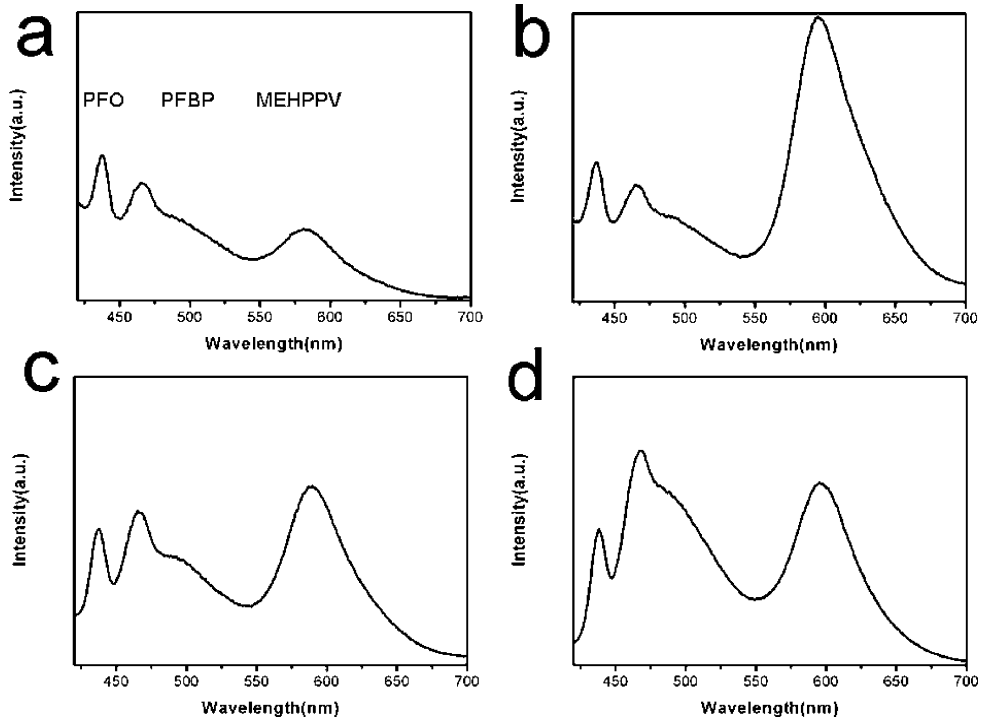

Figure 8. PL emission spectra of barcode nanorods with variable ratios of blue-, green-, and red-emission. Roughly, for examples, PL intensity of PFO:PFBP:MEHPPV = 2:1:1 (a), 2:1:4 (b), 2:1.5:2.5 (c), 2:2.5:2.5 (d).

after the removal of the SiO_2 microspheres and the cleaning procedure (Figure 7c,d). Figure 7 panels e and f display the PL spectra of the nanorods with the blue-, green-, and red-emission peaks. The PL emission peaks matched the original polymer PL emission spectra well with negligible shifts, which suggested that the polymers maintained the same fluorescent characteristics before and after the RIE process.

For the decoding process, although the PL emission from each single layer of the barcoding nanorods may become hard to be distingishable when its thickness is smaller than half of its emission wavelength, the relavtive PL intensity of three colors is measurable. The characteristics of fluorescent barcoding patterns can reflect the composition of the corresponding nanorods. Here, the number of possible fluorescent barcodes that can be generated is only limited by the amount of spectrally distinguishable polymers and the relative PL intensity levels. The ratio of PL intensity of the barcode nanorods is determined by both the loading amount and the quantum yields of different polymers which were fixed in this work. Thus we can control the relative PL intensity ratios by tuning the amounts of polymers in each layer through the spin-coating process. For example, at a certain spin-coating speed, we kept the concentration of one polymer (PFO) constant (5 mg/mL), and changed the concentration of the other polymers (PFBP and MEHPPV) from 5 mg/mL to 15 mg/mL. Therefore, barcode nanorods with different relative fluorescence intensity ratios were fabricated. Fluorescent spectra readouts from the ternary nanorods with different ratios of the blue-, green-, and red-emission polymers were illustrated in Figure 8. Using the fluorescence intensity of PFO as reference, the relative peak intensities followed the amounts of the corresponding polymers in the nanorod arrays, clearly demonstrating the programmability of our barcoding strategy.

In addition to using colors to encode data, the different RIE etching rates of the three polymers also enable shape encoding. We can simply "write" the code just by adjusting the bar width. We found the etching rate of these three polymers were given by PFBP > MEHPPV > PFO. That is, with the same etching development time, the bar width of three layers were in the decreasing order of PFO > MEHPPV > PFBP (Figure 7a, c and b, d). Integrating both color-encoding and shape-encoding, we can greatly enhance the diversity of our barcoding nanorods.

Another way to improve the barcoding capacity of our nanorods is to increase the number of segments. By alternating spin-coating of PFBP and PFO for three cycles with inert PVA layer between them, a six-layered fluorescent polymer film on the substrate was obtained. After the RIE process, six-segmented nanorods were fabricated (Figure 9a). After the removal of the SiO_2 microspheres, upright multisegmented nanorods were shown in Figure 9b. Increasing the compositions of the polymers and the segments, more resolvable codes can be achieved, which demonstrated the versatility of our system.

Harvesting Monodisperse Barcoding Colloidal Particles with Specific Structure. Microarrays exploit positional encoding to carry out large numbers of analyses in parallel but

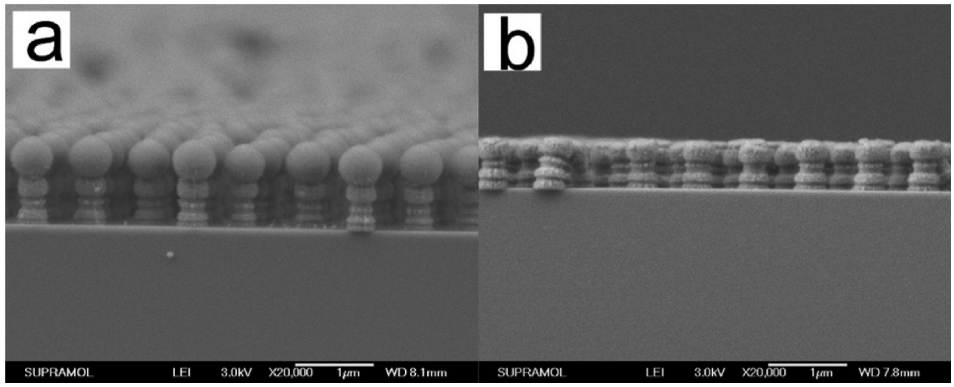

Figure 9. SEM section images of the six-segmented PFO/$(PFBP/PFO)_2$/PFBP (top to bottom) nanorod arrays with silica microspheres (a) and after removal of the silica microspheres (b).

suffer from slow diffusion of analytes to the surface and limitations of simultaneous detection of multiple analytes with low concentrations.[43,44] For this reason, the as-prepared nanorods need to be detached from the substrate. The substrate was changed from silicon wafers to glass slides. During the process of removing

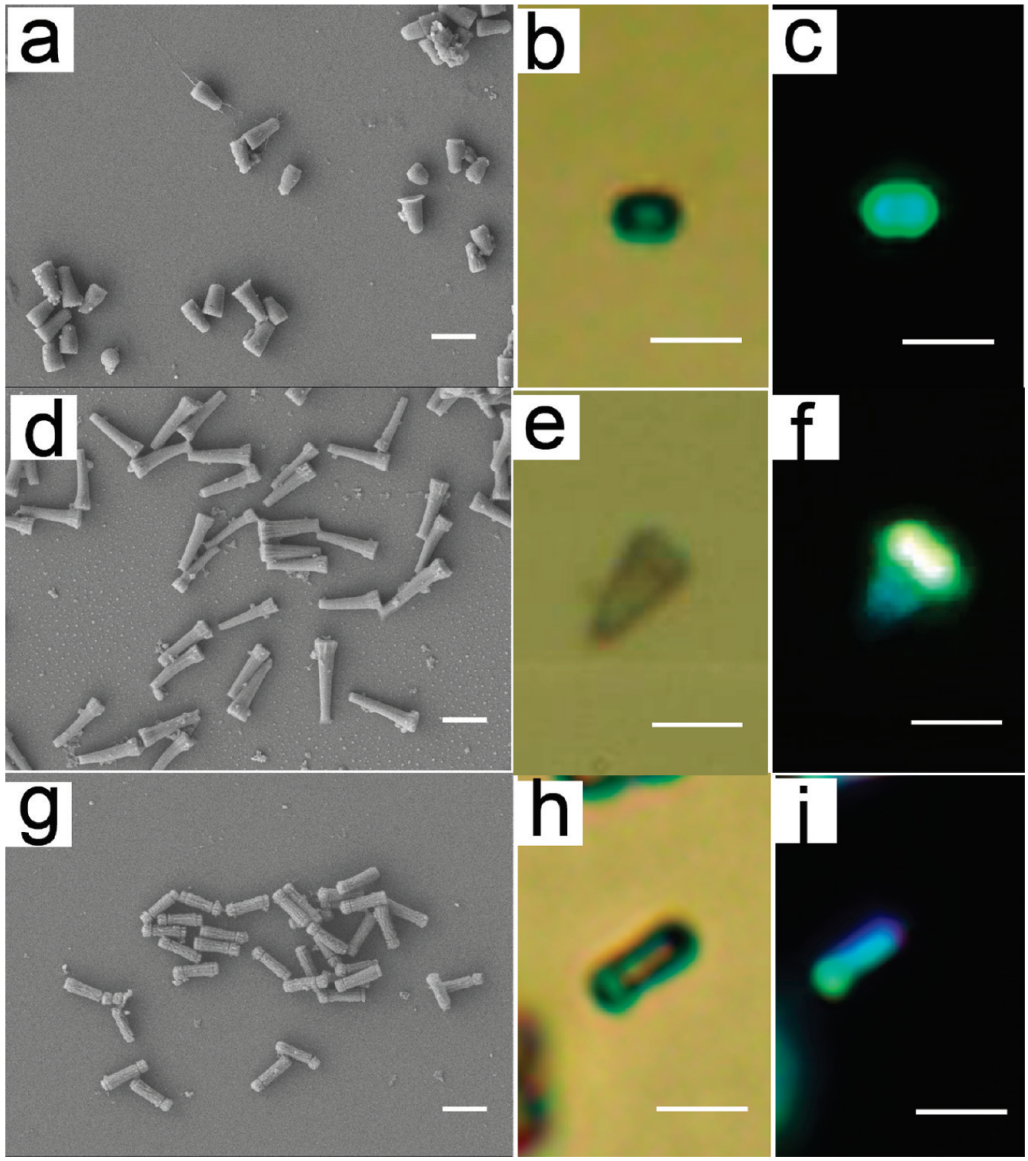

Figure 10. SEM, optical, and fluorescent images of detached PPV nanorods (a, b, c), PPV/PPV@PVA nanorods (d, e, f), and MEHPPV/PFO/PFBP nanorods (g, h, i). All scale bars are 1 μm.

the microspheres with HF, the surface of glass substrate was also dissolved simultaneously and the fluorescent nanorods were released into water. Compared with the nanorod arrays, there is no significant change in PL emission spectra of the suspension, which matched the original polymer PL emission spectra well (Supporting Information, Figure S1). After repeated centrifugations and redispersions, the suspension was drop-coated on a silicon substrate. Figure 10 panels a−c, d−f, and g−i show the SEM, optical, and fluorescence images of the free-standing single-, double-, and triple-segmented nanorods, respectively. These fluorescent nanorods showed good shape retention after the releasing and cleaning processes. A very narrow length distribution at around 890, 1500, and 1080 nm for dispersed single-, double-, and triple-segmented nanorods were observed, respectively. Our measurements from hundreds of nanorods indicated that the size of released fluorescent nanorods remained unchanged compared with the original segment structures on the substrate. Moreover, the PL emission spectra of detached nanorods on substrate, as that of the nanorod arrays and suspension, matched the PL emission of original polymers well, which demonstrated the consistency and controllability of our experimental procedures (Supporting Information, Figure S2).

It is worth noticing here that one of the key advantages of our method is the intrinsic simplicity involved in the delicate control of nanorod fluorescence. We are able to confirm the tunability by observing fluorescence from each layer of our barcoding nanorod using fluorescent microscopy. As shown in Figure 10, the same exposure conditions were applied here, but a different color coding was produced, that is, PPV emit in green, PPV@PVA emit in blue, MEHPPV emit in red, PFO emit in blue, and PFBP emit in green. The colors as well as the approximate profiles of the pattern were successfully reproduced after releasing, as indicated from the microscopy images.

CONCLUSIONS

We described a new strategy to fabricate fluorescent microarrays and multisegmented barcode nanorods *via* RIE using ncp microsphere arrays as shadow masks. The encoding information of these novel barcode nanorods can be easily tuned by adjusting the thickness and sequences of different fluorescent polymer layers, as well as the number of layers. Moreover, the barcode nanorods can be easily detached from their substrates to form a dispersion of coding materials. Such a library of color encoding nanorods could be very useful for the study of geometric and chemical anisotropic effects on product tracking and biodetection. Future developments will greatly benefit from the introduction of novel geometries and from the coupling of distinct patterns for readouts.

EXPERIMENTAL SECTION

Materials. Monodispersed silica microspheres (560 nm) were prepared in ethanol according to the Stöber method.[45] A drop of 10−20 μL of colloidal suspension was applied to the slightly tilted substrate to form colloidal crystals with control over temperature and ambient humidity. Silicon (100) wafers were cleaned by immersion into a solution of H_2SO_4:H_2O_2 (v/v, 7/3) for about 5 h at 90 °C, and then rinsed with a large amount of distilled water and dried by nitrogen gas. Poly(dimethylsiloxane) (PDMS) elastomer kits (Sylgard 184) were purchased from Dow Corning (Midland, MI). PFBP (MW, 12000) was synthesized by the Ma group. MEH-PPV (MW, 40000−70000) and PFO (MW, 70000−1500000) were purchased form Aldrich and American Dye Source separately. Hydrofluoric acid, sulfuric acid, hydrogen peroxide, poly(vinyl alcohol) (PVA), and ethanol were used as received.

Fabrication of Nanorod Microarrays. A schematic illustration of the experimental procedure is shown in Figure 1. Briefly, 0.3 wt % aqueous solution of the precursor polymer (poly(*p*-xylene tetrahydrothiophenium chloride)) of PPV was spin-coated on a silica substrate at a spinning speed of 2000 rpm and a spinning time of 60 s. The film was heated at fixed length at 300 °C under nitrogen for 2 h to convert to PPV. Subsequently, the PDMS stamp was brought into conformal contact with the colloidal film and hot-pressed. By utilizing the lift-up method previously reported,[33] 2D hexagonal close-packed colloidal microsphere arrays were transferred onto the surface of PDMS. After a deformation of PDMS swelled by immerging into toluene for 5 min, close-packed microsphere arrays became nonclose-packed arrays, and then were transferred onto the surface of PPV using a modified microcontact printing reported previously.[34] These ncp arrays were used in colloidal lithography as masks for reactive ion etching. For the RIE process, the oxygen plasma was delivered by a commercially available etching machine (Oxford Plasmalab 80 Plus RIE) including an inductively coupled plasma source (ICP). The following plasma parameters were applied: O_2, 50 sccm; ICP power, 300 W; RF power, 30 W; total pressure, 10 mTorr (1 Torr ≈ 133.3 Pa); nominal substrate temperature, 20 °C. After the RIE process was performed as described above for 2.5 min, the wafer was immersed into HF (6%) to dissolve the silica microspheres, and patterned PPV arrays were obtained.

Fabrication of the Multisegmented Nanorod Arrays. Two-layer films of PPV (bottom) and PVA@PPV (top) were fabricated by successively spin-coating onto the same silica substrate: first, PPV precursor, which was converted to PPV at 300 °C under nitrogen for 2 h; then PVA@PPV with the mass proportion 99:1 PVA to PPV precursor in water, were heated at 150 °C under nitrogen for 2 h. After performing RIE with a colloidal mask, two-segmented nanorod arrays were obtained. Two trilayer-polymer systems were examined: PFBP/PFO/MEHPPV and PFO/PFBP/MEHPPV, which were fabricated by successively spin-coating. First, a 10 mg/mL solution of each polymer in chloroform and a 1 wt % aqueous solution of PVA were prepared. Then a ∼50 μL drop of each solution was spun cast (3000 rpm, 30 s) onto freshly cleaned silica surfaces. To avoid the diffusion of solvent into the previous polymer film, we coated a PVA layer between every two fluorescent polymer layers. Namely, we coated MEHPPV from chloroform first, PVA from water second, PFO from chloroform third, PVA from water fourth, and, PFBP from chloroform fifth onto the same silica substrate as described above. After each spin coating, the single layer film was dried under vacuum at 70 °C for 0.5 h to remove the remnant solvents after spin-coating. The average thickness of the PVA film was 8 nm according to atomic force microscopy measurements, which has negligible effects on the thickness of the resulting trilayer film. Subsequently, a large-area monolayer of nonclose-packed silica microspheres was transferred to the surface of the trilayer film and used in colloidal lithography as masks for reactive ion etching. After the RIE

process was performed as described above for 6 min, the patterned trisegmented nanorod arrays were obtained. Six-layered fluorescent polymer film PFO/$(PFBP/PFO)_2$/PFBP were obtained by spin-coating the solutions of PFBP and PFO alternately for three cycles with inert PVA layer between them. After the RIE and HF etching process mentioned above, six-segmented nanorod arrays were fabricated.

Collection of Free-Standing Polymeric Nanorods. The whole experiment was conducted on a glass substrate. The developed glass substrate was placed in a clean plastic dish containing 30 mL of 5 wt % hydrofluoric acid for 30 s, and the nanorods were released from the wafer *via* dissolution of the glass surface. The suspension of nanorods was placed in 1.5 mL of polypropylene centrifuge tubes. A first centrifugation was performed at 16000*g* for 3 min and the particles were redispersed by sonication in 50 μL of water. The 50 μL suspensions were then combined in one 1.5 mL centrifuge tube. This wash process was repeated three times. The solution of particles was drop-coated on a silica substrate for the microscopy studies.

Characterization. SEM images were taken with a JEOL FESEM 6700F electron microscope with primary electron energy of 3 KV, and samples were sputtered with a layer of Pt (*ca.* 2 nm thick) prior to imaging to improve conductivity. UV−vis adsorption spectra were taken using a Shimadzu 3100 UV−vis−NIR spectrophotometer. True-color fluorescence images were obtained by using an inverted Olympus microscope (BX-51) equipped with a digital color camera and a broad-band ultraviolet (330−385 nm) light source (100-W mercury lamp). Fluorescence experiments were performed by a Shimadzu RF-5301 PC spectrofluorimeter.

Acknowledgment. This work was supported by the National Natural Science Foundation of China (Grant Nos. 20921003, 20874039) and the National Basic Research Program of China (2007CB936402). The author also thanks Prof. Y. G. Ma and Dr. Z. M. Wang for providing fluorescent polymer PFBP.

Supporting Information Available: PL emission spectra of detached barcode nanorods in solution and PL emission spectra of trisegmented barcode nanorods in different forms. This material is available free of charge *via* the Internet at http://pubs.acs.org.

REFERENCES AND NOTES

1. Han, M.; Gao, X.; Su, J. Z.; Nie, S. Quantum-Dot-Tagged Microbeads for Multiplexed Optical Coding of Biomolecules. *Nat. Biotechnol.* **2001**, *19*, 631–635.
2. Wilson, R.; Cossins, A. R.; Spiller, D. G. Encoded Microcarriers for High-Throughput Multiplexed Detection. *Angew. Chem., Int. Ed.* **2006**, *45*, 6104–6117.
3. Nicewarner-Pena, S. R.; Freeman, R. G.; Reiss, B. D.; He, L.; Pena, D. J.; Walton, I. D.; Cromer, R.; Keating, C. D.; Natan, M. J. Submicrometer Metallic Barcodes. *Science* **2001**, *294*, 137–141.
4. Finkel, N. H.; Lou, X.; Wang, C.; He, L. Peer Reviewed: Barcoding the Microworld. *Anal. Chem.* **2004**, *76*, 352A–359A.
5. Liu, F.; Lee, J. Y.; Zhou, W. J. Template Preparation of Multisegment PtNi Nanorods as Methanol Electrooxidation Catalysts with Adjustable Bimetallic Pair Sites. *J. Phys. Chem. B* **2004**, *108*, 17959–17963.
6. Walton, I. D.; Norton, S. M.; Balasingham, A. Particles for Multiplexed Analysis in Solution: Detection and Identification of Striped Metallic Particles Using Optical Microscopy. *Anal. Chem.* **2002**, *74*, 2240–2247.
7. Keating, C. D.; Natan, M. J. Striped Metal Nanowires as Building Blocks and Optical Tags. *Adv. Mater.* **2003**, *15*, 451–454.
8. Qin, L. D.; Park, S.; Huang, L.; Mirkin, C. A. On-Wire Lithography. *Science* **2005**, *309*, 113–115.
9. Piraux, L.; George, J. M.; Despres, J. F.; Leroy, C.; Ferain, E.; Legras, R.; Ounadjela, K.; Fert, A. Giant Magnetoresistance in Magnetic Multilayered Nanowires. *Appl. Phys. Lett.* **1994**, *65*, 2484–2486.
10. Lee, J. H.; Wu, J. H.; Liu, H. L.; Cho, J. U.; Cho, M. K.; An, B. H.; Min, J. H.; Noh, S. J.; Kim, Y. K. Iron−Gold Barcode Nanowires. *Angew. Chem.* **2007**, *46*, 3663–3667.
11. Sioss, J. A.; Keating, C. D. Batch Preparation of Linear Au and Ag Nanoparticle Chains *via* Wet Chemistry. *Nano Lett.* **2005**, *5*, 1779–1783.
12. Qin, L. D.; Banholzer, M. J.; Millstone, J. E.; Mirkin, C. A. Nanodisk Codes. *Nano Lett.* **2007**, *7*, 3849–3853.
13. Seo, D.; Yoo, C. Il; Jung, J.; Song, H. Ag−Au−Ag Heterometallic Nanorods Formed through Directed Anisotropic Growth. *J. Am. Chem. Soc.* **2008**, *130*, 2940–2941.
14. Salem, A. K.; Chen, M.; Hayden, J.; Leong, K. W.; Searson, P. C. Directed Assembly of Multisegment Au/Pt/Au Nanowires. *Nano Lett.* **2004**, *4*, 1163–1165.
15. Ling, X. Y.; Phang, I. Y.; Reinhoudt, D. N. Supramolecular Layer-By-Layer Assembly of 3D Multicomponent Nanostructures *via* Multivalent Molecular Recognition. *Int. J. Mol. Sci.* **2008**, *9*, 486–497.
16. Wang, J. Barcoded Metal Nanowires. *J. Mater. Chem.* **2008**, *18*, 4017–4020.
17. Skinner, K.; Dwyer, C.; Washburn, S. Selective Functionalization of Arbitrary Nanowires. *Nano Lett.* **2006**, *6*, 2758–2762.
18. Bauer, L. A.; Reich, D. H.; Meyer, G. J. Selective Functionalization of Two-Component Magnetic Nanowires. *Langmuir* **2003**, *19*, 7043–7048.
19. Sattayasamitsathit, S.; Burdick, J.; Bash, R. Alloy Nanowires Bar Codes Based on Nondestructive X-ray Fluorescence Readout. *Anal. Chem.* **2007**, *79*, 7571–7575.
20. Banu, S.; Birtwell, S.; Galitonov, G.; Chen, Y.; Zheludev, N.; Morgan, H. Fabrication of Diffraction-Encoded Microparticles Using Nanoimprint Lithography. *J. Micromech. Microeng.* **2007**, *17*, S116–S121.
21. Broder, G. R.; Ranasinghe, R. T.; She, J. K.; Banu, S.; Birtwell, S. W.; Cavalli, G.; Galitonov, G. S.; Holmes, D.; Martins, H. F. P.; MacDonald, K. F.; *et al*. Diffractive Micro-Bar-Codes for Encoding of Biomolecules in Multiplexed Assays. *Anal. Chem.* **2008**, *80*, 1902–1909.
22. Dejneka, M. J.; Streltsov, A.; Pal, S.; Frutos, A. G.; Powell, C. L.; Yost, K.; Yuen, P. K.; Muller, U.; Lahiri, J. Rare Earth-Doped Glass Microbarcodes. *Proc. Natl. Acad. Sci. U.S.A.* **2003**, *100*, 389–393.
23. Grondahl, L.; Battersby, B. J.; Bryant, D.; Trau, M. Encoding Combinatorial Libraries: A Novel Application of Fluorescent Silica Colloids. *Langmuir* **2000**, *16*, 9709–9715.
24. Battersby, B. J.; Bryant, D.; Meutermans, W.; Matthews, D.; Smythe, M. L.; Trau, M. Toward Larger Chemical Libraries: Encoding with Fluorescent Colloids in Combinatorial Chemistry. *J. Am. Chem. Soc.* **2000**, *122*, 2138–2139.
25. Yin, Y. D.; Lu, Y.; Xia, Y. N. A Self-Assembly Approach to the Formation of Asymmetric Dimers from Monodispersed Spherical Colloids. *J. Am. Chem. Soc.* **2001**, *123*, 771–772.
26. Cao, Y. C.; Jin, R.; Mirkin, C. A. Nanoparticles with Raman Spectroscopic Fingerprints for DNA and RNA Detection. *Science* **2002**, *297*, 1536–1540.
27. Lee, J. A.; Mardyani, S.; Hung, A. Toward the Accurate Read-out of Quantum Dot Barcodes: Design of Deconvolution Algorithms and Assessment of Fluorescence Signals in Buffer. *Adv. Mater.* **2007**, *19*, 3113–3118.
28. Tan, W. B.; Huang, N.; Zhang, Y. Ultrafine Biocompatible Chitosan Nanoparticles Encapsulating Multicoloured Quantum Dots for Bioapplications. *J. Colloid Interface Sci.* **2007**, *310*, 464–470.
29. Pregibon, D. C.; Toner, M.; Doyle, P. S. Multifunctional Encoded Particles for High-Throughput Biomolecule Analysis. *Science* **2007**, *315*, 1393–1396.
30. Kim, S. H.; Jeon, S. J.; Jeong, W. C. Optofluidic Synthesis of Electroresponsive Photonic Janus Balls with Isotropic Structural Colors. *Adv. Mater.* **2008**, *20*, 4129–4134.
31. Fournier-Bidoz, S.; Jennings, T. L.; Klostranec, J. M.; Fung, W.; Rhee, A.; Li, D.; Chan, W. C. W. Facile and Rapid One-Step Mass Preparation of Quantum-Dot Barcodes. *Angew. Chem.* **2008**, *120*, 5659–5663.

32. Kuang, M.; Wang, D. Y.; Bao, H. B. Fabrication of Multicolor-Encoded Microspheres by Tagging Semiconductor Nanocrystals to Hydrogel Spheres. *Adv. Mater.* **2005**, *17*, 267–270.
33. Yao, J.; Yan, X.; Lu, G.; Zhang, K.; Chen, X.; Jiang, L.; Yang, B. Patterning Colloidal Crystals by Lift-up Soft Lithography. *Adv. Mater.* **2004**, *16*, 81–84.
34. Yan, X.; Yao, J. M.; Lu, G.; Li, X.; Zhang, J. H.; Han, K.; Yang, B. Fabrication of Non-Close-Packed Arrays of Colloidal Spheres by Soft Lithography. *J. Am. Chem. Soc.* **2005**, *127*, 7688–7689.
35. Koh, S. J. Controlled Placement of Nanoscale Building Blocks: Toward Large-Scale Fabrication of Nanoscale Devices. *J. Occup. Med.* **2007**, *59*, 22–28.
36. Herold, M.; Gmeiner, J.; Schwoerer, M. Influence of the E-Limination Temperature on Light Emitting Devices Prepared from Poly(*p*-phenylene vinylene). *Acta Polym.* **1996**, *47*, 436–440.
37. Chen, B.; Wei, J.; Tay, F. E. H.; Wong, Y.; Iliescu, C. Silicon Microneedle Array with Biodegradable Tips for Transdermal Drug Delivery. *Microsyst. Technol.* **2008**, *14*, 1015–1019.
38. Finkel, N. H.; Prevo, B. G.; Velev, O. D. Ordered Silicon Nanocavity Arrays in Surface-Assisted Desorption/Ionization Mass Spectrometry. *Anal. Chem.* **2005**, *77*, 1088–1095.
39. Schubert, D. W.; Dunkel, T. Spin Coating from a Molecular Point of View: Its Concentration Regimes, Influence of Molar Mass and Distribution. *Mater. Res. Innovations* **2003**, *7*, 314–321.
40. Schubert, D. W. Spin Coating as a Method for Polymer Molecular Weight Determination. *Polym. Bull.* **1997**, *38*, 177–184.
41. Bjorklund, T. G.; Lim, S. H.; Bardeen, C. J. The Optical Spectroscopy of Poly(*p*-phenylene vinylene)/ Polyvinylalcohol Blends: From Aggregates to Isolated Chromophores. *Synth. Met.* **2004**, *142*, 195–200.
42. Reiss, B.; Freeman, R.; Walton, I.; Norton, S.; Smith, P.; Stonas, W.; Keating, C. D.; Natan, M. J. Electrochemical Synthesis and Optical Readout of Striped Metal Rods with Submicron Features. *J. Electroanal. Chem.* **2002**, *522*, 95–103.
43. Nolan, J. P.; Sklar, L. A. Suspension Array Technology: Evolution of the Flat-Array Paradigm. *Trends Biotechnol.* **2002**, *20*, 9–12.
44. Braeckmans, K.; De Smedt, S. C.; Leblans, M.; Pauwel, R.; Demeester, J. Encoding Microcarriers: Present and Future Technologies. *Nat. Rev. Drug Discovery* **2002**, *1*, 447–456.
45. Stöber, W.; Fink, A.; Bohn, E. Controlled Growth of Monodisperse Silica Spheres in the Micron Size Range. *J. Colloid Interface Sci.* **1968**, *26*, 62–69.